Using First Principles Density Functional Theory
Methods to Model the
Seebeck Coefficient of Bulk Silicon

by

Saahil Mehra

Submitted to the Department of Materials
Science and Engineering in Partial
Fulfillment of the Requirements for the
Degree of

Bachelor of Science

at the

Massachusetts Institute of Technology

May 2008
[June 2008]

Signature of Author.....
Department of Materials Science and Engineering
May 16, 2008

Certified by .....
Gerbrand Ceder
R. P. Simmons Professor of Materials Science and Engineering
Thesis Supervisor

Accepted by .....
Caroline Ross
Chairwoman, Undergraduate Thesis Committee

Abstract:

Thermoelectrics are gaining significant amounts of attention considering their relevance today in the areas of sustainable energy generation and energy efficiency. In this thesis, the thermoelectric properties of bulk Silicon were modeled using *ab initio* density functional theory methods to determine the Si band structure. Specifically, three different models for determining the Seebeck coefficient – Parabolic Bands, Boltzmann's theory, and the 'Pudding Mold' approximation to Boltzmann's theory – were studied in depth and compared with experimental values. Here we show first principles calculations to yield Seebeck coefficients for n-type Silicon to be on the order of 300 μV/K at –300 K, and –500 μV/K at 300 K for the Parabolic Bands and Boltzmann approach, respectively. While the 'Pudding Mold' Theory failed in its approximations of the Seebeck coefficients, the calculations using the other two theories were found to agree closely with experimentally determined Seebeck coefficients.

Acknowledgements:

I would like to thank MIT, the DMSE, Professor Ceder and his group for the direction provided and the access to the necessary resources to perform the work entailed in this project. Specifically, Maria Chan was of great help and I really would not have been able to do this thesis without her guidance and feedback. Without her, this thesis would not have been.

TABLE OF CONTENTS:

I. Introduction:

The search for sustainable energy sources and a solution to the international energy dilemma have become some of the greatest concerns regarding our future. Global economic, environmental, and social pressures are pushing us to change how we harness and utilize vital energy, and these pressures will increase over the next few decades as we expand to an estimated population of ten billion people by mid-century [1]. Environmental impacts of global warming and climate change are already affecting living species, increasing the urgency with which these solutions need to be delivered [2]. With electricity generation projected to double by 2030, there exists a huge gap in generating capacity that needs to be filled. Moreover, the issue of climate change has become a real and very significant concern, with greenhouse gas emissions increasing and the Earth's average temperature having increased more than a degree in the last 100 years [3].

A useful method to contribute to the sustainable generation movement is the use of thermoelectric generators to utilize waste heat in various situations, including automobiles, homes, as well as manufacturing & industrial processes. Thermoelectrics are devices that use temperature gradients to generate electricity, or alternatively transport heat when an electrical current is run through them. The field of thermoelectric materials has recently received significantly more attention as efforts are being made to improve automobile fuel efficiency by replacing alternators with thermoelectric generators, for example [4]. However, for thermoelectric devices to reach their full potential, novel materials need to be developed that allow for higher performance, lighter weight thermoelectric devices.

In this thesis project, three different approaches used to calculate the Seebeck coefficient – a key factor in optimizing thermoelectric materials performance – were evaluated using first principles Density Functional Theory. The goal of this thesis is to understand from a theoretical perspective the important properties for thermoelectric energy conversion and how they are determined.

II. Motivation

Silicon was chosen as a material to model due to its widespread usage in electronic and integrated circuit applications. As a result, despite its high thermal conductivity, the fact that processing of silicon is a simple, reproducible, well established technology makes it useful for low power systems [5]. Recently, low dimensional silicon nanowires have been touted as potential new thermoelectric materials with lowered thermal conductivities and higher figures of merit [6]. Crystalline silicon assumes a diamond cubic crystal structure with two atoms in each of the unit cell and four symmetrically placed covalent bonds. As a result, each silicon unit cell has 8 valence electrons. The silicon band gap has been experimentally determined and accepted to be 1.12 eV [7].

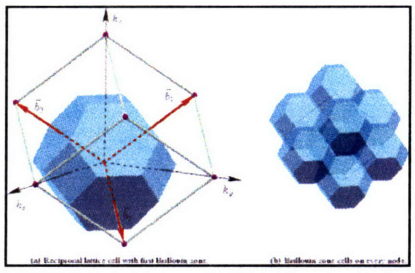

Figure I: The first Brillouin zone for diamond structure silicon – the Wigner-Seitz cell for the reciprocal lattice. The depiction on the right shows the periodicity of the silicon Brillouin zone cells. Figure adapted from [8].

III. Background:

In a thermoelectric material, free carriers in the material carry both charge and heat. An applied temperature gradient causes charged carriers in the material, electrons and holes, to diffuse across the temperature gradient, giving rise to an electric potential. This is known as the Seebeck effect. The thermopower, or Seebeck coefficient, is given by the ratio of potential gradient to temperature gradient. The ideal thermoelectric material would have a large thermopower, a low thermal conductivity, and a high electrical conductivity. Materials development focuses on increasing values of zT, the thermoelectric figure of merit, to increase the overall conversion efficiencies.

$$ZT = \frac{\alpha^2 T}{\rho\kappa}$$

In this equation, α is the Seebeck coefficient in V/K, T is temperature in K, ρ is the electrical resistivity, and κ is the thermal conductivity. Each of these parameters is dependent on interconnected material properties, which makes it difficult to optimize zT in a material. Values of $zT \approx 1$ are considered to be good and attaining values of $zT \approx 3$-4 is considered a key step for thermoelectrics to compete as a power generation medium [6].

The four main variables that need to be engineered in thermoelectric materials are the carrier concentrations, the effective mass, as well as the electronic and lattice thermal conductivities. To maximize the voltage generated by a temperature gradient, one needs to maximize the number of carriers using only one type of charge. Good thermoelectric materials are often heavily doped semiconductors with a carrier concentration between 10^{19} and 10^{21} cm^{-3}. Effective mass of the charge carrier provides another conflict as large effective masses produce high thermopower but low electrical conductivity [9]. Thus, a balance must be obtained between maximizing effective

mass and carrier mobilities. Thermal conductivity manifests itself in two ways in thermoelectric materials, with electrons and holes transporting heat as well as phonons traveling through the lattice. Good thermoelectric materials must scatter phonons without disrupting electrical conductivity. Unfortunately, an offset due to thermal conductivity exists due to its direct relation to the electronic conductivity as per the Wiedemann-Franz Law [10].

IV. Computational Methods – Density Functional Theory:

a. Background:

The Schrodinger Equation defines a relation for which all the information of a system of N electrons is stored within the wave function, Ψ. Whether a system is an atom, a solid, or a molecule depends only on the external potential, $v(\mathbf{r})$. For systems with more than two electrons – a many body problem – the Schrodinger equation can not be solved analytically.

$$\left[\sum_{i}^{N}\left(\frac{\hbar^2}{2m}\nabla_i^2 + v(r_i)\right) + \sum_{i<j} U(r_i, r_j)\right]\Psi(r_1, r_2 \dots r_N) = E\,\Psi(r_1, r_2 \dots r_N)$$

Computational requirements to solve the Schrodinger equation for an N electron system scale with N^N to represent Ψ in **k**-space, which is far beyond any practical computing capabilities. As a result, there have been many attempts to reduce the computational intensity of these calculations using different approximations and assumptions.

Density Functional Theory (DFT) allows the mapping of the many-body problem with interacting electrons to a single body problem, assuming electrons don't interact, and using the particle density as the key variable [11]. In using DFT, the complicated many body electronic

wave-function is substituted by the simpler electronic density, overcoming the fundamental limitations in dealing with many electron systems. The Hohenberg-Kohn Theorem asserts that an external potential uniquely determines the ground state charge density, and the charge density uniquely determines the external potential.

$$n(r) \Leftrightarrow \Psi(r_1, r_2 \ldots r_N) \Leftrightarrow v(r)$$

All effects of exchange and correlation are included in a term in the total energy functional. The Generalized Gradient Approximation (GGA) uses the local charge density at a given point but also takes into account the gradient of the charge density when approximating the exchange-correlation energy [12]. Minimizing the total energy functional leads to a set of Schrodinger-like equations with an explicit effective potential known as the Kohn-Sham equations. The Kohn-Sham equations provide a practical way to approximate the density functional for real systems [12].

b. Implementation:

In practice, pseudopotentials are used to reduce computational intensity by assuming that electrons in the inner atomic shells are so tightly bound that they are not perturbed by the external environment. The Kohn-Sham equations are solved numerically by representing the electronic wave-functions as a linear combination of a set of plane wave basis functions [13]. The use of plane wave basis sets allows the wave function to be expressed in terms of reciprocal space vectors within the 1st Brillouin zone of the periodic cell – now the Brillouin zone just needs to be sampled at a defined set of **k**-points and the Kohn-Sham equations solved.

The algorithm for implementing DFT to determine the charge density is as follows [14]. First, we take initial guesses for $n^{\downarrow}(\boldsymbol{r})$, $n^{\uparrow}(\boldsymbol{r})$ and use that to calculate the effective potential. Once the effective potential is determined the electron density is recalculated and tested using criteria for convergence. This process occurs iteratively until the convergence criterion is satisfied.

V. Calculations:

All calculations were done using Plane Wave Self-Consistent Field (PWscf), an open source computer code for electronic structure calculations within DFT. For the bulk silicon sample, a self-consistent calculation was first performed to determine the ground state charge density. The Brillouin zone was sampled at 256 **k**-points using an 8x8x8 **k**-point mesh, which was determined to be sufficient for convergence of the ground state charge density.

Once the ground state charge density had been determined, a non-self consistent field calculation (NSCF) was performed to determine the band structure of the bulk Si in the first Brillouin zone. The NSCF calculation required a much finer grid of **k**-points to be used to accurately approximate the band energies and shape across the reciprocal lattice space. As a result, a 50x50x50 **k**-point mesh was used to survey the Brillouin zone in steps of 0.02. The pseudopotential used for both calculations was the Perdew-Burke-Enzerhof exchange correlational functional (GGA), with a nonlinear core correction and the Vanderbilt ultrasoft potential to ensure smooth transition of wave function at the core radius. All post-processing of the output band energies was done using MATLAB software. The data was stored and the algorithms to calculate each of the properties were written and implemented entirely within MATLAB.

VI. Results and Discussion:

a. Part 1: Validation of Theory

Here we will present the results obtained from post-processing of the PWscf output for the band energies and use the relevant information to perform calculations. The resulting band energies for each of the first eight energy bands in the 1st Brillouin zone for bulk silicon were output by PWscf for each of the k-points sampled.

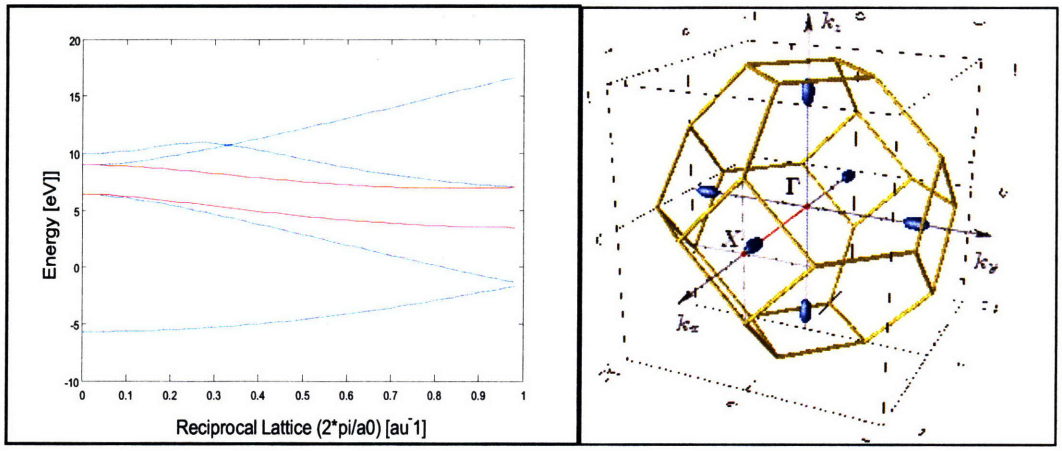

Figure 2: Band diagram across the 1st BZ for bulk Si, as calculated using PWscf. The higher and lower energy red bands correspond to the lowest conduction and highest valence bands, respectively. It is observed that the valence band maximum occurs at gamma point, where the conduction band minimum occurs at ~0.84*(2*pi/a0) [a.u] in the b_1 reciprocal lattice direction. The plot of the Brillouin zone corresponds to the Δ-line, which is marked by the red line in the figure on the right. Adapted from [8].

Semiconductor band structures are difficult to describe with an analytical formula. The plot is drawn for energy values along particular edges of the irreducible wedge of the Brillouin zone, with the energy dispersion along a straight line form the point Γ to point X. The band gap of Si was calculated to be 0.54 eV, which is slightly more than a 50% error from the experimentally determined band gap of 1.12 eV. DFT is known for its error in calculating band gaps in materials. For the conduction band, the minima lie on the <100> direction and occur roughly 85% of the way to the 1st Brillouin zone boundary.

The next step was to calculate the curvature of the valence and conduction bands at the band extrema, to determine the electron and hole effective mass tensors and ratios. The effective mass is a key property in solid state physics and for thermoelectric, as larger effective masses produce larger thermopowers but compromise electrical conductivity [6]. From a thermoelectric standpoint, it is important to use materials that optimize the effective mass with regard to both of the measurements. From the band structure, the effective mass tensor and ratios are expressed as

$$m^*_{\alpha\beta} = \left(\frac{1}{\hbar^2}\frac{\partial^2 \varepsilon}{\partial k_\alpha \partial k_\beta}\right)^{-1} \qquad \frac{m^*_{\alpha\beta}}{m_e} = \left(m_e \frac{1}{\hbar^2}\frac{\partial^2 \varepsilon}{\partial k_\alpha \partial k_\beta}\right)^{-1}$$

where m_e is the rest electron mass, and $\frac{\partial^2 \varepsilon}{\partial k_\alpha \partial k_\beta}$ is the band curvature for a given α and β direction. The band curvature was approximated using finite differences and the Central Difference Theorem, which allowed the determination of the effective masses at the valence band maximum (holes) and conduction band minimum (electrons). The tensors were diagonalized to yield the effective masses in the three principal directions, m^*_{XX}, m^*_{YY}, & m^*_{ZZ}.

m*/m at Valence band maximum		
-0.2658	0	0
0	-0.2658	0
0	0	-0.2658

m*/m at Conduction band minimum		
0.9667	0	0
0	0.1936	0
0	0	0.1936

Tables 1 & 2: Diagonalized effective mass tensors for the valence and conductions bands (holes and electrons). These are found to agree with experimental DFT values for silicon extremely well, with m^* for holes calculated to be 0.26 and m^* for electrons calculated to be 0.96 (longitudinal) and 0.16 (transverse) [15].

Despite the relative coarseness of the **k**-point mesh used for these calculations, we observe effective mass values extremely close to those calculated previously using DFT as well as

experimental values for the electron effective mass ratios – 0.9163 (longitudinal) and 0.1905 (transverse) [16]. The symmetry of the effective mass tensor across gamma is attributed to the crystal symmetry in the x-, y-, and z- directions of reciprocal lattice space whereas the asymmetry in the electron effective mass tensor is explained by the variation in the conduction band curvature in different axes directions in **k**-space. As a result, the anisotropy of the effective mass with respect to crystal orientation can play a large role in maximizing the thermopower in silicon.

The intrinsic carrier concentrations and temperature dependence were calculated as a validation check to verify the model's capability to describe experimental values that are well known in the field. The Fermi function,

$$f(\varepsilon(\boldsymbol{k})) = \frac{1}{1 + \exp\left(((\varepsilon(\boldsymbol{k}) - \mu))/k_B T\right)}$$

which describes the probability of occupation of a certain temperature, was summed over all of the k-points in the 1st Brillouin zone for each band to determine the occupation levels. The gamma energy of the valence band was taken to be the reference Fermi level for all hole concentration calculations, while the minimum of the conduction band was used as the reference level for electron concentrations. For the hole concentration calculations, the number of holes in the lower four bands was equal to the difference between the number of electrons expected to occupy the first four energy bands of Si – 8 – and the number of electrons calculated to be in each band for a given temperature.

$$N_n^{holes} = 8 - \frac{2}{N_k} \sum_{k_x} \sum_{k_y} \sum_{k_z} f(\varepsilon_n(\boldsymbol{k}))$$

Every point on each band (every n,**k**), was summed for its contribution to the total electron and hole concentration since it was observed that bands 2, 3, 4 were all degenerate at the Gamma point and thus had to be accounted for in each of the calculations.

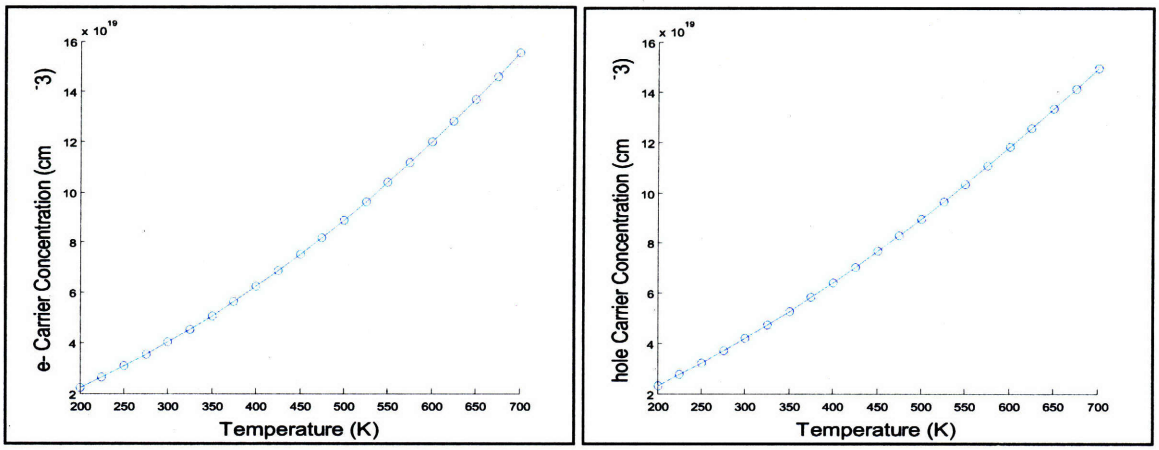

Figure 3: Electron and Hole concentrations varying temperature from 200 to 700 K.

These numbers were found to be in general agreement with previous calculations, which have been previously calculated for electrons for chemical potential at the conduction band minimum to be 3.2×10^{19} cm^{-3} [17]. Using PWscf results were found to be very close, as electron carrier concentrations of 4×10^{19} cm^{-3} were calculated for 300 K. Likewise, for hole carrier concentrations the calculated values also were on the same order of magnitude with those observed in the literature, 1.8×10^{19} cm^{-3} [17]. Carrier concentrations on the order of $10^{18} - 10^{21}$ in thermoelectric materials have been found to optimize both the electrical conductivity and thermal conductivities [6]. The errors associated with these calculations are can be attributed to the sparseness of the k-point mesh used, which resulted in crude approximations of the Fermi function and undervalued the carrier concentrations at each temperature.

Additionally, the relationships between the carrier concentrations and chemical potential were plotted, and it was observed that shifting the chemical potential slightly into the band gap resulted in lower occupations for both electrons and holes.

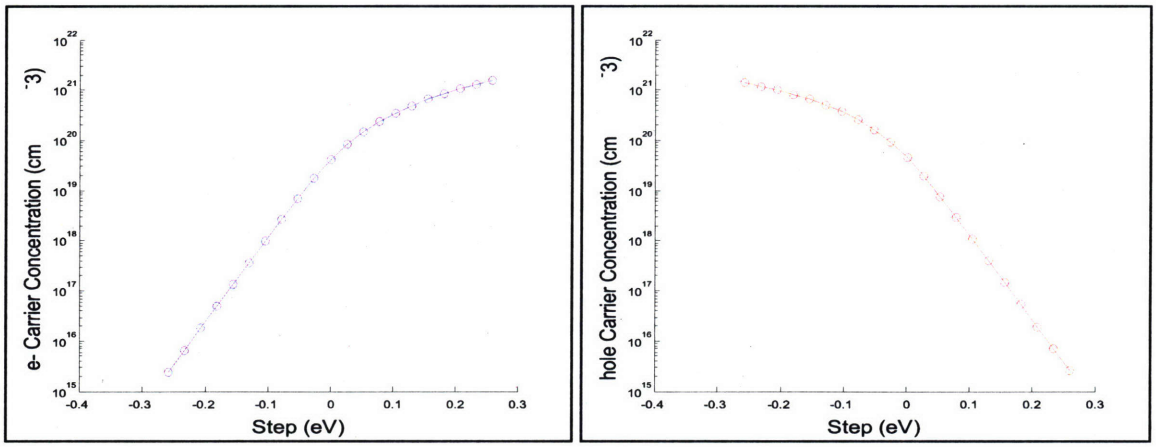

Figure 4: Electron and Hole concentrations vs. steps in the chemical potential. It is observed that increases in the chemical potential resulted in higher concentrations for electrons and lower concentrations for holes.

Figure 4 shows how the carrier concentrations varied with an energy step from the valence band maximum and conduction band minimum for holes and electrons, respectively. For higher values of the chemical potential the carrier concentrations for electrons are seen to increase as the Fermi function overlaps with a larger portion of the electron density of states. On the other hand, here it is observed that increasing the chemical potential results in decreasing hole concentrations due to a decrease in the overlap between the Fermi function and hole density of states.

To calculate the conductivity tensor, calculations were performed using the equation [10]

$$\sigma_{\alpha\beta}(\varepsilon(\boldsymbol{k})) = e^2\,\tau(\varepsilon(\boldsymbol{k}))\iiint v_\alpha(\boldsymbol{k})\,v_\beta(\boldsymbol{k})\frac{\partial f(\varepsilon(\boldsymbol{k}))}{\partial\varepsilon(\boldsymbol{k})}\,d\boldsymbol{k}_x d\boldsymbol{k}_y d\boldsymbol{k}_z$$

where τ is the relaxation time & v_α and v_β are the velocities given by $\frac{1}{\hbar}\frac{\partial\,\varepsilon(k)}{\partial k}$. The relaxation time was assumed to be constant at 10^{-14} s [18] and the velocities were calculated using finite

differences between band energies at each k-point. $\frac{\partial f(\varepsilon(k))}{\partial \varepsilon(k)}$ is the derivative of the Fermi function, expressed analytically as

$$\frac{\partial}{\partial \varepsilon(k)} f(\varepsilon(k)) = \frac{-\exp\left((\varepsilon(k)-\mu)/k_B T\right)}{k_B T \left(1+\exp\left((\varepsilon(k)-\mu)/k_B T\right)\right)^2}$$

Conductivity calculations for the holes were summed over all the occupied bands at each point in the **k**-point mesh. To determine the relationship between the conductivity and the carrier concentrations, the carrier concentration was calculated using different Fermi Energies at a given temperature, and the Fermi Energy was shifted by an energy step, δ for multiple values. Similarly, the conductivities were calculated by varying the Fermi Energy with the same energy step and δ was used to parameterize the relationship between the conductivity tensor and the hole carrier concentration.

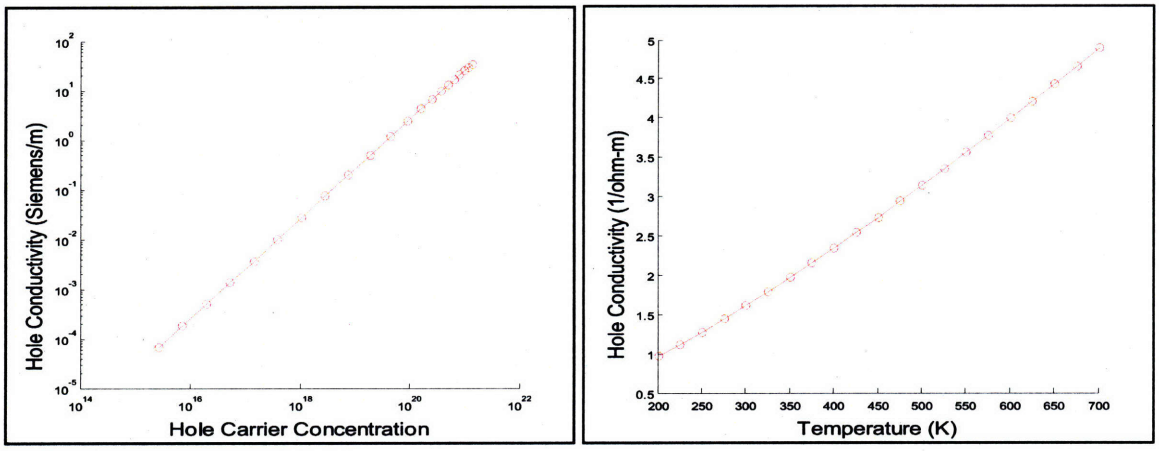

Figure 5: Plots of conductivity vs. concentration for holes and temperature show how conductivity increases in value with larger T and concentrations.

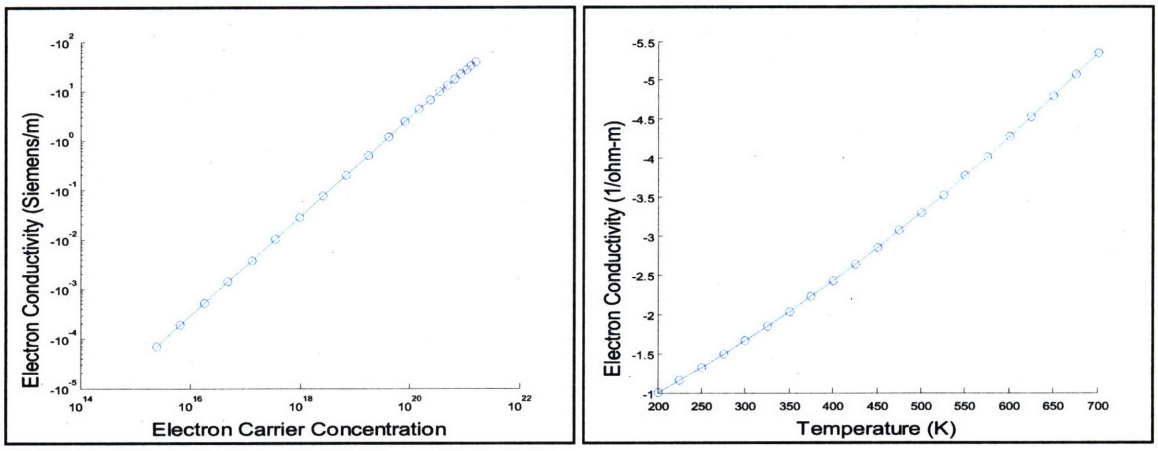

Figure 6: Plots of conductivity vs. concentration for electrons and temperature show how conductivity increases in magnitude with larger T and concentrations.

These results agree with experimental tests and validate the methods used thus far. As a result of increased carrier concentrations and mobilities in experiment, resistivity was experimentally observed to decrease with carrier concentration in accordance with the results [7]. Similarly, increasing temperatures corresponded to higher conductivities, which is indicative of higher concentrations of charge carriers at higher T as a result of the smoothing of the Fermi function. Conductivities for Si have been observed to vary with carrier concentration from 10^{-3} 1/Ohm*m to 10^{-5} 1/Ohm*m [5].

b. Part 2: Comparison of Different Models

i. Parabolic Bands

The conductivities, carrier concentrations, and relations defined in the previous section were applied to test the predictions of three different models for the thermopower. The first one used nearly free electron theory, approximating the electrons in the Si crystal as independent, and assumes that near the valence and conduction band extrema the bands can be modeled as parabolic [10]. In common cubic semiconductors, the bands can be approximated as

$$E(\mathbf{k}) = \frac{\hbar}{2}\left(\frac{k_\ell^3}{m_\ell^*} + \frac{k_t^3}{m_t^*} + \frac{k_t^3}{m_t^*}\right).$$

which describes a band with ellipsoidal constant energy surfaces [8]. This yields an expression for the Seebeck coefficient, α, as

$$\alpha = \frac{8\pi^2 k_b^2}{3eh^2} m^* T \left(\frac{\pi}{3n}\right)^{2/3}$$

predicting a linear dependence on the temperature and inverse carrier concentration dependence [19]. Similar to the conductivity calculations, the factor associated with scattering distance (and scattering time) was assumed to be unity [20]. Using the respective carrier concentrations and effective masses for holes and electrons, the n-type and p-type Seebeck coefficients were calculated with respect to two parameters – varying the temperature and the intrinsic carrier concentration.

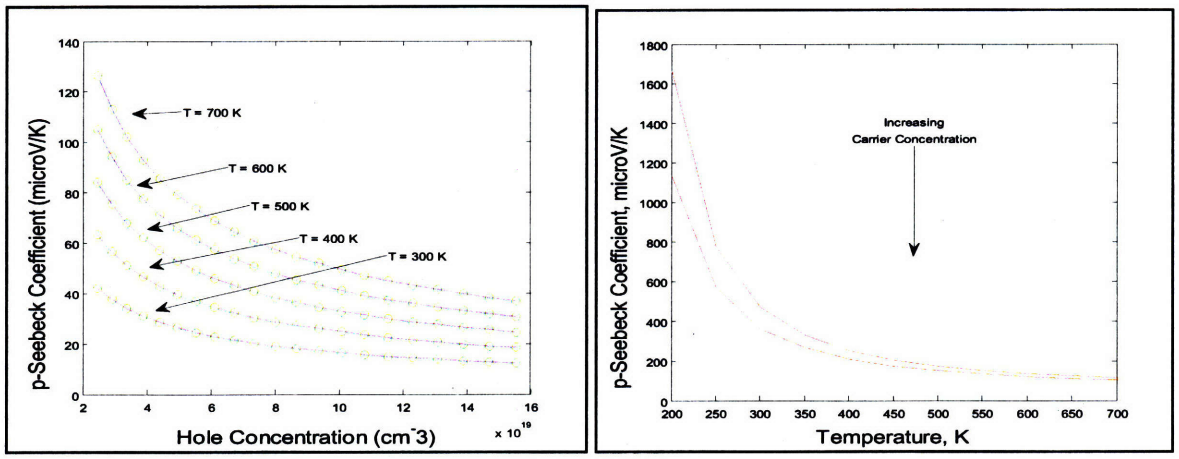

Figure 7: p-type Seebeck coefficient vs. hole concentration and temperature using the Parabolic Bands model. In the left figure the Seebeck coefficient is seen to decrease in magnitude with higher concentrations at fixed temperature. In the right figure, the Seebeck coefficient is plotted with temperature and corresponding carrier concentration. As the carrier concentration increases exponentially while α is linear with respect to T, the Seebeck coefficient decreases with temperature.

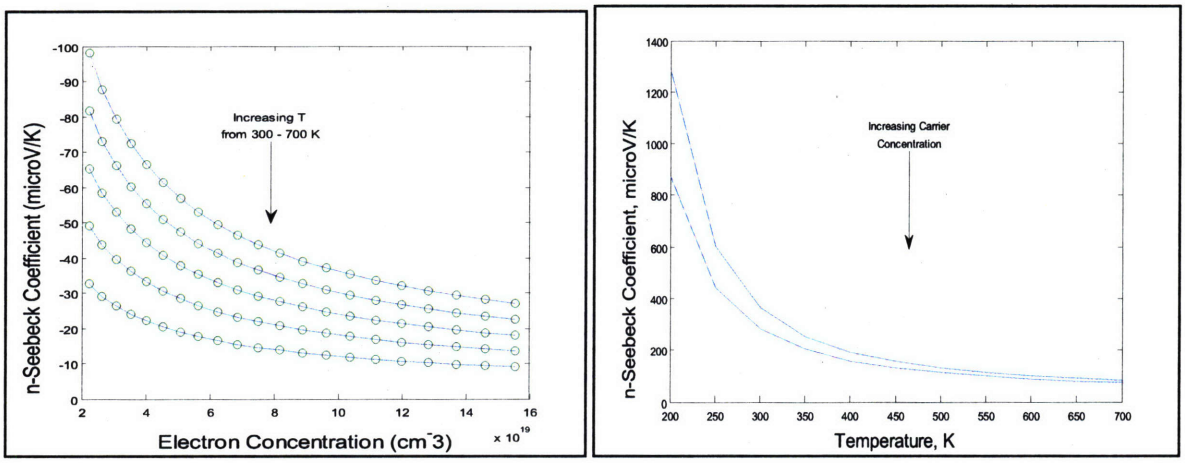

Figure 8: n-type Seebeck coefficient vs. electron concentration and temperature using the Parabolic Bands model.

The calculated results for the thermopower with respect to the temperature and concentration showed the expected trends from the Seebeck equation shown above. At the carrier concentration of 10^{18} cm^{-3} for temperature of 300 K, the Seebeck coefficient for n-type silicon is observed to be on the order of -300 μV/K. These were compared to be in close agreement with degenerate n-type Si of similar carrier concentration at 300 K [21]. The Seebeck coefficient showed a complex relation with temperature. While the equation for the Seebeck coefficient has a direct temperature dependence, the plots show decreasing values of the Seebeck coefficient with increasing temperature. As temperature increases, the carrier concentration increases exponentially but the Seebeck coefficient is proportional to $Tn^{-2/3}$, so a net decrease is expected. This is confirmed by the shape of the graphs of the n- and p-type Seebeck coefficients with respect to the associated carrier concentrations.

These graphs did not completely agree with experimental results, however. Experimental data showed a drop-off, or peak, at 670 K corresponding to the transition between extrinsic and intrinsic carriers [22]. At that point the Fermi function is smoothed to the point where intrinsic carriers are the dominant charge carrying mechanism, which corresponds to a decrease in the

Seebeck coefficient. In the case of parabolic bands plots, which only account for intrinsic carriers, the increasing intrinsic carrier concentration with higher temperatures corresponds directly with the decrease in Seebeck coefficient since these are the only charge carriers and there are no dopants or other extrinsic carriers modeled.

ii. **Boltzmann Approach – Full Theory**

The Boltzmann equation approach to thermopower calculates the Seebeck coefficient as

$$S = \frac{1}{eT} K_0^{-1} K_1$$

where K_n, is given by

$$K_n = \sum_k \tau(k) v(k) v(k) \left[-\frac{\partial f(\varepsilon)}{\partial \varepsilon}(k) \right] (\varepsilon(k) - \mu)^n$$

Again, a constant relaxation time was assumed – which allows the relaxation time to be pulled out of the sum and to cancel in the quotient of $K_0^{-1} K_1$. The temperature and carrier concentration dependence of the n- and p-type Seebeck coefficients are plotted in Figures 9 and 10 for holes and electrons, respectively. It is difficult to predict the temperature dependence prior to simulation, as the inverse temperature factor in the denominator is complicated by the temperature dependence of the Fermi function and its derivative.

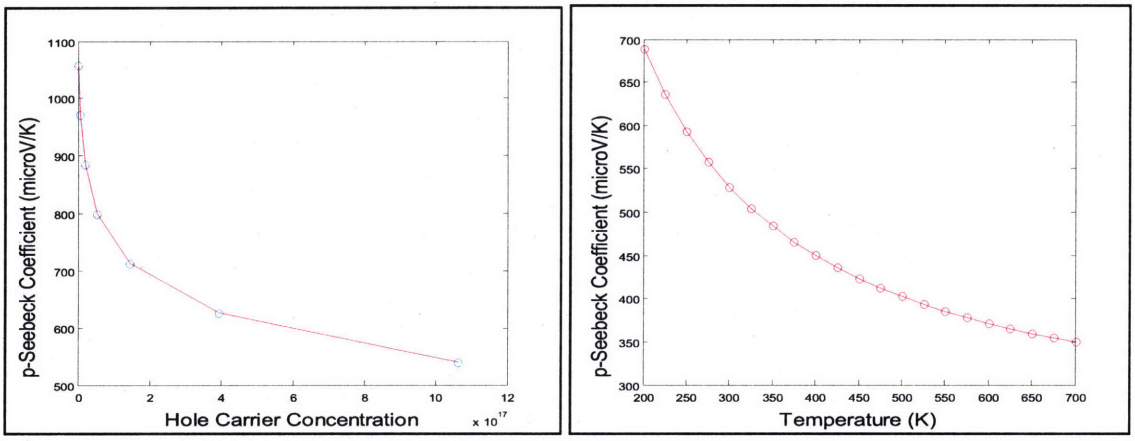

Figure 9: p-type Seebeck vs. hole concentration and temperature using the Boltzmann approach. Decreases in the thermopower are observed with increasing carrier concentration and temperature.

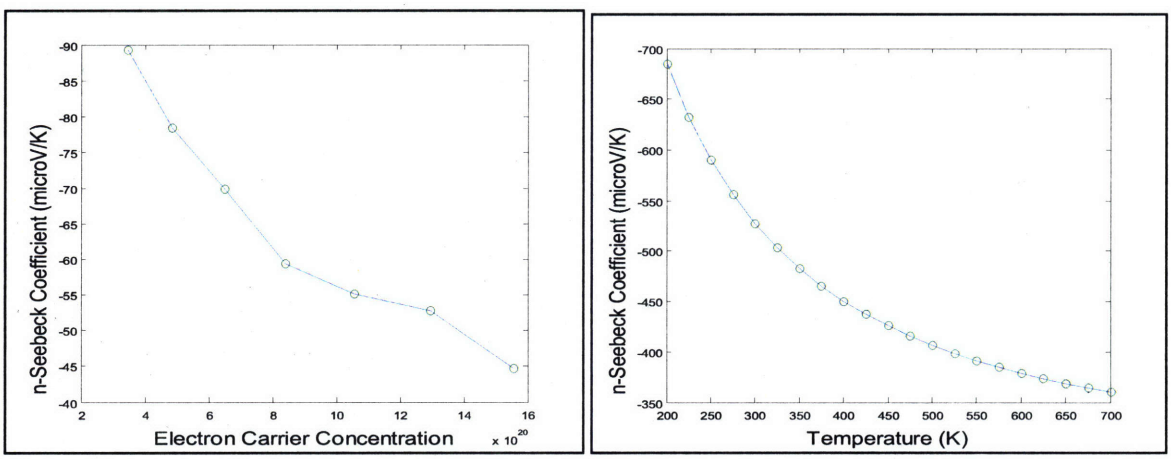

Figure 10: n-type Seebeck vs. electron concentration and temperature using the Boltzmann approach. Decreases in the thermopower are observed with increasing carrier concentration and temperature

The data for the Seebeck coefficients show similar trends observed using the parabolic bands approximation, and in the Full Theory calculations the n-type data follow more closely in magnitude with those observed in Geballe and Hull [21]. Figure 10 shows the n-type Seebeck coefficients to vary between -400 and -700 μV/K, whereas Geballe and Hull observe experimentally for n-type silicon a variation in the Seebeck coefficient from -600 to -750 μV/K in the range of 300-700 K.

iii. Pudding Mold Model:

Lastly, we examine the validity of the Pudding Mold approximation to Boltzmann transport theory applied to bulk silicon. Kuroki et. al. proposed the "Pudding Mold" model as a means to model materials with a particular shape associated with the band dispersion [23]. Taking the assumption that these bands are shaped more like a "pudding mold" than a quadratic (contrary to the Parabolic Bands approximation), the Seebeck coefficient can be approximated by only considering the states with energies within kT from the chemical potential. For the bulk silicon calculations, the reference chemical potential was approximated to be at the valence band maximum for p-type and at the conduction band minimum for n-type and calculations are carried out for T = 300 K.

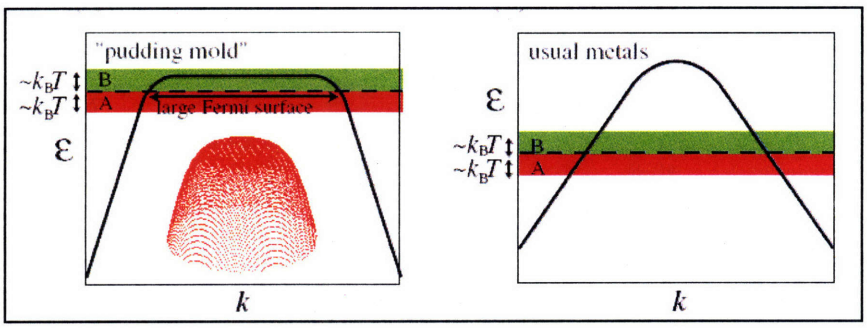

Figure 7: Describes the shape of a "pudding mold" material in contrast with a metal whose bands are effectively parabolic at the extrema. Due to the localized areas of high curvature in the pudding mold model, the states within that energy range contribute significantly more to the electrical and thermoelectric materials properties. Figure adapted from [20].

As shown in Figure 7, the states within O(kT) of the Fermi Energy contribute disproportionately more to the electronic transport properties due to the large variation in curvature and band velocity around that energy. Kuroki et. al. approximate this contribution as

$$K_0 \sim \sum{}'(v_A{}^2 + v_B{}^2) \qquad \boldsymbol{K_1} \sim k_B T \sum{}'(v_A{}^2 - v_B{}^2)$$

where Σ' implies a summation over all the states in the range of $|\varepsilon(\boldsymbol{k}) - E_F| < \sim kT$, and v_A & v_B are the typical velocities for the energy states above and below the fermi Energy. Using these conditions, the relationships for holes and electrons between the Seebeck coefficient vs. carrier concentration and the Seebeck coefficient vs. temperature were calculated and shown in Figures 11 and 12 below.

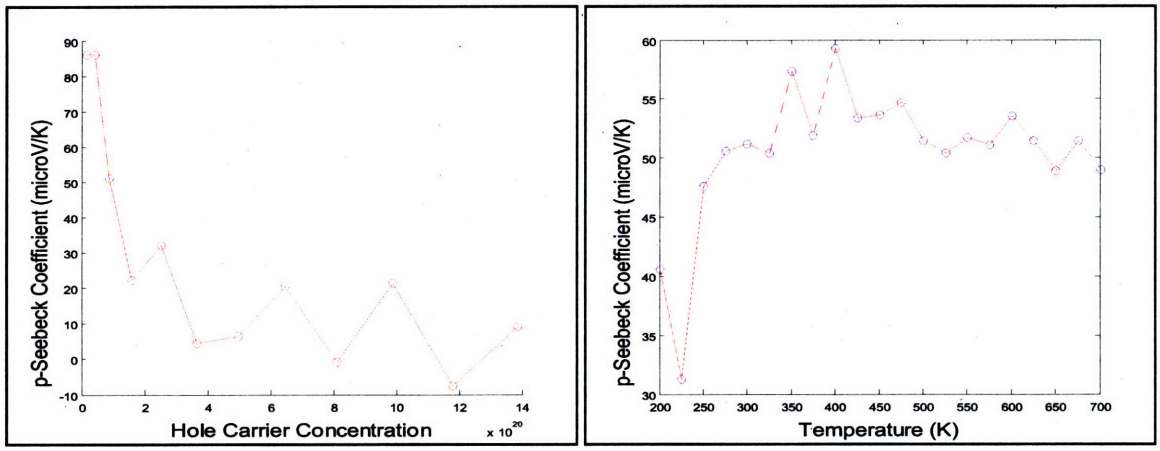

Figure 11: p-type Seebeck vs. hole concentration and temperature using the pudding mold approximation to the Boltzmann approach. Decreases in the Seebeck coefficient are observed with increasing carrier concentration, while the Seebeck coefficient increases in magnitude with increasing temperature.

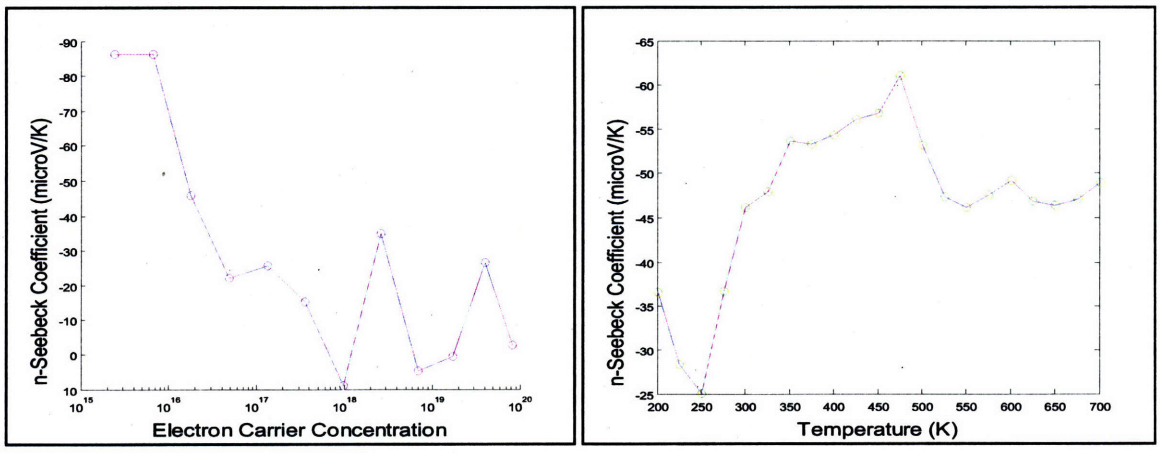

Figure 12: n-type Seebeck vs. electron concentration and temperature using the pudding mold approximation to the Boltzmann approach. Decreases in the Seebeck coefficient are observed with increasing carrier concentration, while the Seebeck coefficient increases in magnitude with increasing temperature.

While the plots of the Seebeck coefficient against the carrier concentrations for holes and electrons show similar trends as the Parabolic Bands and Full Theory approximations, the values

of the Seebeck coefficient are much smaller than those observed experimentally by Geballe and Hull. Additionally, the jagged nature of the plots against both carrier concentrations and temperature for both electrons and holes is a limitation of the model when applied to a **k**-point mesh of insufficient density, since there is a huge variation in the number of states that are calculated when the step across the Brillouin zone is 0.02. Due to the the large step size between each point on the band, the sum of the velocities above and below the Fermi energy varied significantly with each step, resulting in deviations from the expected smooth relation between the two parameters. It is important to note that the calculation of the Seebeck coefficient vs. p-type carrier concentration curve involved a parameterization of the carrier concentration and Seebeck coefficient with chemical potential, and subsequently plotting the relation between the Seebeck coefficient and hole carrier concentration. As a result of the chemical potential being at the valence band maximum, the carrier concentration did not vary over as large of a range.

However, the plots for both n- and p-type Seebeck coefficients against temperature did not reflect the previously observed trends using the Parabolic Bands model and the Full Theory. The limitation of this model is that it approximates K_1 as the difference in band velocities squared between those states above and below the chemical potential within a given energy range. This does not explicitly take into account the changes in occupation as a result of increasing temperature, which calculations using both of the other models did. Increasing the temperature increased the size of the range where values would be accepted to contribute to the Seebeck approximation. While this implicitly selects states within a certain energy range of the chemical potential, it does not account at all for the changes in occupation, which is why the plots against temperature exhibit increases in the magnitude of the Seebeck coefficient with temperature.

c. **Part 3: Error Analysis:**

A major source for the errors in magnitude in this thesis was the result of the coarseness of the k-point mesh used to approximate the band structure. The mesh of equally spaced steps in the first Brillouin zone of reciprocal lattice space of 0.02 did not afford the type of precision necessary for accuracy of calculations that depend on the order 10^{-5}, such as calculating the number of electrons and holes in each band. Two areas where the **k**-point mesh density considerations adversely affected the calculation precision were in determining the number of electrons in each of the occupied bands as well as taking the Fermi function derivative in the conductivity calculations. In the calculations over the number of occupied bands, the total number of electrons in each band was calculated by summing the Fermi function valued at each k-point for each of the occupied bands and normalizing this number by the total number of **k**-points used in the calculation.

$$N_e = \frac{2}{N_k} \sum_{k_x} \sum_{k_y} \sum_{k_z} f(\varepsilon(\boldsymbol{k})) = \frac{2}{N_k} \sum_{k_x} \sum_{k_y} \sum_{k_z} \frac{1}{1 + \exp\left((\varepsilon(\boldsymbol{k}) - \mu)/k_B T\right)}$$

For a sparse **k**-point mesh, the number of electrons calculated using this method will have significant error due to the small number of values contributing to the sum. For steps of 0.02 across the 1st Brillouin zone, the error associated with this did result in variations in the carrier concentration (and subsequently Seebeck coefficient) calculations.

Additionally, errors due to the density of the **k**-point mesh were also observed when writing the algorithm for the conductivity calculations. Conductivity was calculated as sum over all the bands and **k**-points of the product of the group velocities and the Fermi function derivative. The analytical derivative of the Fermi function was shown earlier was found to have serious errors

associated with it. Integration of the Fermi function derivative should yield the Fermi function – or probability of a state being occupied – valued at a particular energy. For many different energies, the integral value of the Fermi function derivative were values greater than one, which is unphysical. The root cause of this was an excessively large step between any two given points on the **k**-point mesh, so the numerical approximation to the integral was often significantly overvalued.

As a result, a major reason why these calculations all displayed the correct general trends but often had large percentage errors was the density of the **k**-point mesh used for the band structure calculations. As is the problem in computational materials science, there is always a trade off between efficiency and accuracy. The results obtained in this project here are significant enough to explain the physical phenomena that are occurring but need to be redone for a more accurate band structure calculation to get more precise numbers.

VII. **Conclusion:**

In this thesis project, the band structure and thermoelectric properties of silicon were calculated using first principles Density Functional Theory. Three different models for the Seebeck coefficient were examined closely and compared with experimental values in literature. The data and calculations showed that the general trends were satisfied for both the Parabolic Band and Boltzmann Approach, but many discrepancies were observed when comparing the n- and p-type Seebeck coefficients calculated using the "Pudding Mold" approximation to the Boltzmann Theory with those observed experimentally.

The Boltzmann approach yielded the most accurate calculation of the Seebeck coefficient vs. carrier concentrations, while the Parabolic Bands approximation did as well. Using the Parabolic Bands the values calculated were on the same order of magnitude as those experimentally observed but were somewhat smaller, owed partially due to miscalculated carrier concentrations again as a result of the **k**-point mesh density. However, the "Pudding Mold" approximation also showed jagged graphs due to its inability to extract general trends from **k**-point grids that were insufficiently dense. Furthermore, the model is limited in its applicability because it would not explicitly account for changes in the occupation. The Parabolic Band and Pudding Mold approximations are effectively opposite in their approaches, as one attempts to model the bands at their extrema as parabolic while the other – the 'Pudding Mold' approach – assumes the valence and conduction bands are effectively flat at their extrema.

A more thorough study of these models and how these models vary quantitatively can be undertaken but would require significantly more computational time and a denser grid of **k**-points to accurately reflect the band structure of these materials. Additionally, further studies could be pursued to examine the electronic structure of strained silicon grown on SiGe to gain insight into the electronic structure and fundamental mechanisms behind the favorable electronic properties attributed to strained Si [24].

References:

1. Bradford, Travis. Solar Revolution: the Economic Transformation of the Global Energy Industry. Cambridge, MA: The MIT Press, 2006.
2. Camille, Parmesan, and Yobe, Gary. "A Globally Coherent Fingerprint of Climate." Nature 421 (2003): 37-43. 5 Mar. 2008.
3. United States. DOE. Climate Change. 3. March 2008 <http://www.energy.gov/environment/climatechange.htm>.
4. DiSalvo, F. J. Thermoelectric cooling and power generation. Science 285, 703–706 (1999).
5. Glosch, H et. al. "A Thermoelectric Converter for Energy Supply" Sensors and Actuators 74 (1999) 246-250
6. Snyder, J. and Toberer, E. "Complex Thermoelectric Materials" Nature Materials 7 (2008) 105-113
7. Seto, John Y.W. "The Electrical Properties of Polycrystalline Silicon Films" Journal of Applied Physics 46 12 (1975) 5247-5253
8. Wessner, Wilfried. "Mesh Refinement Techniques for TCAD Tools" PhD Dissertation – Technischen Universität Wien. 19 February 2008. < http://www.iue.tuwien.ac.at/phd/wessner/diss.html>
9. Rowe, D. M. (ed.) CRC Handbook of Thermoelectrics: Macro to Nano (CRC, Boca Raton, 2005).
10. Ashcroft, N. & Mermin, D. "Solid State Physics" Textbook – Harcourt Brace College Publishers (1976)
11. Hohenberg, P. and Kohn W., "Inhomogeneous Electron Gas" Phys. Rev. 136, B864 (1964)
12. Kohn. W, "Nobel Lecture: Electronic Structure of Matter – wave functions and Density functional", Rev. Mod. Phys. 71 5 (1999)
13. Eichler, Andreas "Sampling the Brillouin Zone" Lecture - Universit¨at Wien – Accessed 19 April 2008 http://cms.mpi.univie.ac.at/vasp-workshop/
14. Perdew, J. & Kurth, S. " Density Functionals for Non-relativistic Coulomb Systems in the New Century", Lecture Notes in Physics – Springer Berlin 500 (1998)

15. Bulusu, A. & Walker, D.G "Modeling of Thermoelectric Properties of Semiconductor Thin Films with Quantum and Scattering Effects" Journal of Heat Transfer 129 (2007) 491-498
16. Hensel, J.C .et. al "Cyclotronic Resonance in Uniaxially Stressed Silicon. II. Nature of the Covalent Bond" Phys. Rev. 138 (1965)
17. Shur, M., "Physics of Semiconductor Devices", Textbook-Prentice Hall, 1990.
18. Van Arsdale, Jack. "Interaction of 10.6-micron Radiation with bulk Silicon" Defense Technical Information Center <http://stinet.dtic.mil> (1968) Accessed 21 March 2008
19. Cutler, M. et. al "Electronic Transport in Semimetallic Cerium Sulfide" Phys. Rev. 144 4A (1964) A1143-A1151
20. Cutler, M, Leavy J.F, Fitzpatrick R.L , Phys. Chem. Solids 24 319 (1963)
21. Geballe, T. & Hull, G "Seebeck Effect in Silicon" Phys. Rev. 98 4 (1955)
22. Fulkerson, W. et. al "Thermal Conductivity, Electrical Resistivity, and Seebeck Coefficient of Silicon from 100 to 1300 K" Phys. Rev. 167 **3** (1968) 765-781
23. Kuroki, K. and Arita, R. "'Pudding Mold' Band Drives Large Thermopower in NaxCoO2" Jour. Phys. Soc. Japan 76 8 (2007)
24. Lee, M. & Fitzgerald, E. "Strained Si, SiGe, and Ge channels for high-mobility metal-oxide-semiconductor field-effect transistors" Journ. Applied Physics 97 (2005)